

A novel acceleration criterion for remote-end grounding-fault in MMC-MTDC under communication anomalies

Ning Tong¹, Zhenjie Tang¹, Chun Sing Lai^{1,2}, Xue Li³, Alfredo Vaccaro⁴, Loi Lei Lai¹

1. School of Automation, Guangdong University of Technology, Guangzhou 510006, PR China

2. Brunel Interdisciplinary Power Systems Research Centre, Brunel University London, London UB8 3PH, UK

3. School of Electromechanical Engineering, Guangdong University of Technology, Guangzhou 510006, PR China

4. Department of Engineering, University of Sannio, Italy

*l.l.lai@gdut.edu.cn

Abstract:

The multi-terminal HVDC system based on the modular multilevel converter (MMC-MTDC) has very high technical merits for long-distance, flexible power transmission. In recent years, there has been a significant improvement in developing its fast-speed primary protection, especially for local-measurement-based ones immune to communication anomalies. However, in many cases, the problem of remote-end fault identification for the local-measurement-based protection elements needs further studies, mainly because such protection elements should balance between sensitivity and security. This paper proposes a novel acceleration criterion to identify remote-end faults for the MMC-MTDC. Based on the difference of the traveling wave propagation characteristics between the scenario of internal faults and that of the external fault, the local-end protection element will detect a highly-oscillating signal due to the opening of the remote-end DC circuit breaker. In contrast, no such signal will be observed in the external fault scenario. The wavelet time entropy is utilized to quantify the feature of oscillation. The performance of the proposed criterion is assessed based on the established four-terminal MMC-MTDC on the PSCAD/EMTDC platform. Results indicate that by using the proposed criterion, the sensitivity of the local-measurement-based protection element against remote-end faults is greatly enhanced.

Index Terms: MMC-MTDC, traveling wave, DC circuit breaker, fault sensitivity

Nomenclature

<i>Abbreviations</i>			
AC	Alternative Current	t_{in}^1/t_{in}^2	The main/second wave arriving time (Internal fault conditions)
DC	Direct Current	Δt_{out}	The arriving time difference of external faults
CB	Circuit Breaker	Δt_{in}	The arriving time difference of internal faults
CLR	Current-Limiting Reactor	V_{Iwb}	The main wave generated by faults
WTE	Wavelet-Time Entropy	V_{Iwf}	The forward wave generated by faults
DWT	Discrete Wavelet Transform	V_{2wb}	The second wave generated by DC CB opening
MOA	Metal Oxide Arrester	f	The frequency of internal fault oscillation waves
MMC	Modular Multilevel Converter	f'	The frequency of external fault oscillation waves
MTDC	Multi-Terminal DC system	f_m	The theoretical maximum detectable frequency
HVDC	High-Voltage DC transmission system	γ	The sampling rate
HVAC	High-Voltage AC transmission system	ε	The absolute dead-zone
H-MMC	Half-bridge Modular Multilevel Converter	$x(t)$	A continuous signal for the wavelet transform
WFPDL	Wave-Front Protection for DC line-to-ground fault	$\psi(t)$	The basis of wavelet function
		$D_h(t)$	The component of scale h for wavelet calculation
		h	The number of scales of wavelet decomposition
		s	The stretch factor
		ω	The length of the sliding window
		σ	The sliding step
		S_0/S_L	Minimum/maximum indicators
		p_z	The probability indicator to calculate WTE
		H_{WTE}^h	The calculated WTE of scale- h
		Z_l	The l -th interval for WTE calculation
		N	The total number of points for WTE calculation
		n_z	The number of points in a sub-zone
		τ	The main aerial-/zero-mode wave-arrival time difference
		$\tau_1/\tau_2/\tau_3$	Setting values for τ to decide fault scenarios
		$\Delta u_0/\Delta u_1$	Superimposed zero-/aerial-mode voltage
		$\Delta i_0/\Delta i_1$	Superimposed zero-/aerial-mode current
		S_{0_set}	WFPDL zero-mode wave setting value
		S_{1_set}	WFPDL aerial-mode wave setting value
		ΔS_{0_set}	WFPDL zero-mode differential setting value
<i>Symbols</i>			
Z_0/Z_1	The zero-/aerial-mode wave impedance		
u_1	The aerial-mode forward traveling wave		
u_{1r}/u_{1l}	Aerial-to-aerial refraction/reflection wave		
R_g	The fault resistance		
Λ_{11}/Γ_{11}	Aerial-to-aerial reflection/refraction coefficient		
l/l'	The length of the local/adjacent DC line		
x/x'	Percentage of fault location on local/adjacent line		
v_1	The aerial-mode wave velocity		
T/T'	The cycle of internal/external fault oscillation		
T_b	The delay of DC CB to interrupt a fault		
T_0	The time window of primary protection		
T_d	The time window of WFPDL		
T_m	The critical fault-clearing time		
T_{om}	The maximal calculated period of oscillations		
t_1/t_0	Aerial-/zero-mode main wave arrival times		
t_{out}^1/t_{out}^2	The main/second wave arriving time (External fault conditions)		

I. Introduction

In comparison with conventional high-voltage alternative current (HVAC) transmission systems, the high-voltage direct-current (HVDC) is a promising technology for its high power-transfer capacity, long transmission distance, and flexible control of active power [1-3]. With the acute need for renewable energy integration, bulk power transmission, etc., the MMC-MTDC has witnessed tremendous development [4, 5]. To protect half-bridge MMCs (H-MMCs) equipped in such systems, DC circuit breakers (CBs) are developed and equipped, especially for the isolation of DC line faults. Besides the update of the DC CB-related technologies, there are also very critical requirements for the protective relay because the typical operation time is at most 5-6 ms [6, 7], or the MMC may be blocked due to over-current.

By using remote-end measurements, unit-protection elements are capable of identifying the fault that occurs on the entire length of the DC line. However, for MMC-MTDCs, the speed of such protection elements is far from satisfactory because of the limitations of the communication volume and the time-cost [8]. As a result, the unit-protection element is only employed as a backup [9]. Local-measurement-based protection elements are free of double-end communication and data-synchronization. To make them work as primary protection elements in the MMC-MTDC, a short time window is required to speed up the operation once an internal fault occurs. Also, as far as the sampling rate can be sufficiently high, there will be a significant enhancement for the sensitivity using high-frequency components.

In this field, many have made significant contributions. In [10], a real-time boundary wavelet transform method is proposed for the MMC-MTDC. In comparison with the conventional stationary wavelet transform, the border effects on the wavelet coefficient energy are introduced to solve the problem of time delays associated with long mother wavelets. In [11], a fault detection scheme for MMC-MTDC is proposed to draw transient current harmonics from the initial fault current by using discrete Fourier transform, which overcame the high-resistance fault and faulty pole identification problems. However, the influence of the DC CB operation process is ignored in engineering applications. In [12], based on the difference of frequency response characteristics of boundary elements between internal and external faults, a fault-detection method is proposed using the current ratio of high-to-low-frequency. However, the impact of remote-end faults needs further discussion. In [13], the distributed optical current sensing technology and other auxiliary methods are utilized to improve the reliability performance of differential protection and traveling wave protection. In [14], a non-unit transient boundary protection element is proposed based on a novel synchrosqueezing wavelet transform. In [15], a fast non-unit DC line protection scheme based on fault transient voltage is proposed, with high-speed detection capability and great adaptability. However, there is a high requirement for time accuracy of capturing wave-front to distinguish internal and external faults. In [16], a non-unit DC fault detection method utilizing the transient average value of line current for radial MTDC system is proposed. The impact of wind-energy integration is also considered. In [17], a detection

method using one-end information is proposed based on the difference of the high-frequency fault current components between the faulted line and the healthy line. The impacts of line length and the supplement inductance are analyzed.

In [18], a high-speed traveling-wave protection element is proposed using very short time windows and high-frequency components. The theory has been successfully adopted in the Zhangbei four-terminal MMC-MTDC. However, the universal shortage of the above contributions is that the value of the DC current-limiting-reactor (CLR) equipped at the ends of DC lines has an evident impact on the performance of such protection elements. The setting of CLRs is not to keep the primary protection element sensitive enough but to compromise between the current-limiting capability and the dynamic behavior of the MMC-MTDC [19]. For this reason, the typical value of CLRs is about 150 mH in existing engineering applications. In scenarios where the required resistive tolerance is as high as 300 Ω for 500 kV systems, existing primary protection elements will have a dead zone or a less-sensitive zone, usually located at the remote end where the local-end protection element may fail to trip the fault. This will affect the stability of the MMC-MTDC and even damage the MMC converters. Protection elements using the remote-end acceleration signals perform less satisfactorily because the protection speed will sharply decline with the introduction of remote-end measurements. Moreover, such protection criteria will fail under communication anomalies.

The contribution of this paper is to propose a novel acceleration criterion for existing local-measurement-based primary protection elements, also using merely local measurements. The following issues that existing primary protection elements encounter should be solved: 1) the lack of sensitivity to identifying internal remote-end grounding faults without communication; 2) the lack of speed to isolate the remote-end grounding fault without communication. Correspondingly, the proposed criterion should feature: 1) high sensitivity – in terms of protection elements for 500-kV DC lines, a resistive tolerance of 300 Ω is required under the single-line-to-ground fault condition [20] and 2) adequate speed – tripping the local-end DC CB before the blocking of H-MMC (typically 5 ms). Towards this end, the characteristics of the main traveling wave (caused by the inception of the fault, internal or external) and the second traveling wave (caused by the operating of the remote-end DC CB) are analyzed. The wavelet-time-entropy (WTE) is utilized to quantify the difference between the above two scenarios.

The remainder of this paper is organized as follows. In Section II, the time-domain difference of the second traveling waves between the scenarios of the external fault and the internal dead-zone fault is analyzed theoretically. Section III discusses and introduces the methodology of quantifying the above difference. How does the proposed criterion work to accelerate the dead-zone fault before the blocking of the MMC converter is also illustrated. In Section IV, simulation cases are conducted to evaluate the performance of the proposed criterion. Finally, the contributions are concluded in Section V.

II. Theoretical study

1) Reflection coefficient

Assume that u_1 is the aerial-mode forward traveling wave. Z_0 and Z_1 are zero- and aerial-mode wave impedances, respectively. R_g represents the fault resistance. According to Peterson's law, aerial-to-aerial refraction wave u_{1r} can be deduced by:

$$u_{1r} = \frac{4R_g + Z_0}{4R_g + Z_0 + Z_1} \times u_1 \quad (1)$$

According to Kirchhoff's law, the aerial-to-aerial reflection wave u_{1l} can be obtained by:

$$u_{1l} = u_{1r} - u_1 = -\frac{Z_1}{4R_g + Z_0 + Z_1} \times u_1 \quad (2)$$

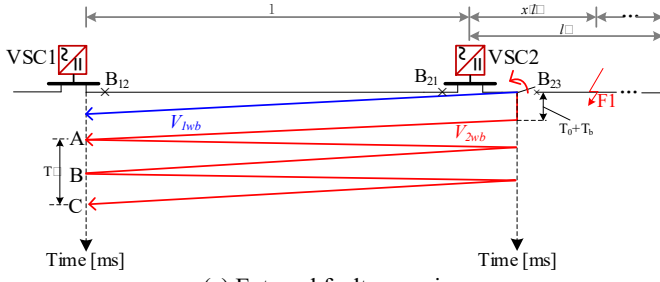
Aerial-to-aerial reflection coefficient Λ_{11} and aerial-to-aerial refraction coefficient Γ_{11} can be written by:

$$\begin{cases} \Lambda_{11} = \frac{u_{1l}}{u_1} = \frac{-Z_1}{4R_g + Z_1 + Z_0} \\ \Gamma_{11} = \frac{u_{1r}}{u_1} = \frac{4R_g + Z_0}{4R_g + Z_0 + Z_1} \end{cases} \quad (3)$$

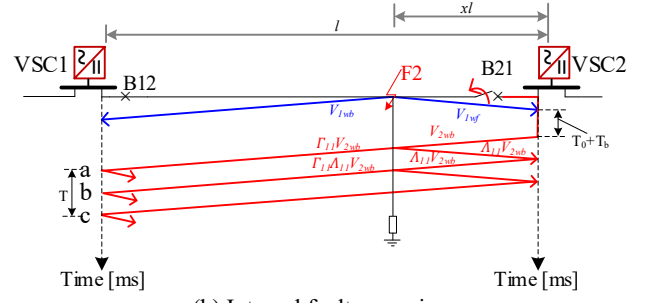
For DC lines, the value of zero-mode wave impedance Z_0 is usually 3~5 times larger than the aerial-mode wave impedance. For this reason, the zero-mode traveling wave has a more evident dispersion effect. In this paper, the influence of zero-mode traveling waves on aerial-mode traveling waves is ignored.

2) Analysis for the different fault scenarios

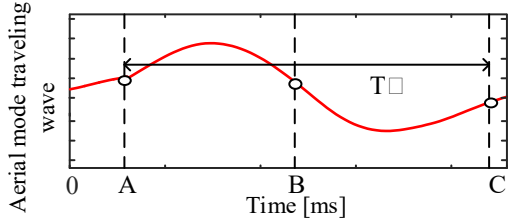
Fig. 1 shows the analysis for the different scenarios between external faults and internal dead-zone faults, where Fig. 1(a) and Fig. 1(b) are the traveling-wave propagation processes of the above two scenarios, and Fig. 1(c) and Fig. 1(d) are the corresponding waveforms. The details are as follows:



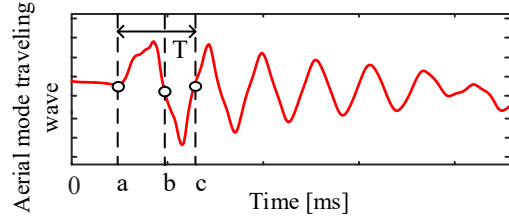
(a) External fault scenarios



(b) Internal fault scenarios



(c) Waveforms of an external fault scenario



(d) Waveforms of an internal fault scenario

Fig. 1 Illustration for the traveling-wave propagation process

External faults

Under external fault conditions, the transient process of traveling wave propagation is shown in Fig. 1(a). In this figure, l is the length of the DC line. x' is the percentage of distance of the adjacent line from the fault point F1 to the near-end protection at the adjacent line. l and l' are the lengths of the local DC line and that of the adjacent line, respectively. v_1 is aerial-mode wave velocity. T_b is the inherent time delay of the opening operation of the DC CB, and T_0 is the time window of the primary protection. The refraction and reflection process of the initial wave caused by an external fault is described below.

First, the occurrence of the fault causes the main wave, starting at the fault location of F1. V_{1wb} passes through the location of B23 and propagates in a reverse direction to the local-line protection at B12. Let the moment when the main wave arrives at B12 be t_{out}^1 . Then, the protection at B23 detects the main wave mentioned above. The fault at F1 is determined as an internal fault (out of dead zone) for the primary

protection located at B23. Thus, this protection element outputs the trip signal, and the DC CB at B23 opens after a delay of $T_0 + T_b$. After that, the second wave V_{2wb} caused by the opening of DC CB B23 propagates along the DC line and arrives at the location of the local-end protection at B12.

Let the moment of the second wave arrival at B12 be t_{out}^2 . According to the transient process of external fault traveling wave propagation, the moments of the main wave arrival, the second wave arrival, and the time difference of Δt_{out} can be deduced by:

$$\begin{cases} t_{out}^1 = \frac{x'l' + l}{v_1} \\ t_{out}^2 = \frac{x'l' + l}{v_1} + T_0 + T_b \\ \Delta t_{out} = t_{out}^2 - t_{out}^1 = T_0 + T_b \end{cases} \quad (4)$$

From Equation (4), it is evident that when an external fault occurs, the local protection detects that the time difference between the arrival of the main traveling wave and the second wave is a certain value T_0+T_b . The second wave V_{2wb} will be reflected repeatedly between the line boundary at B₁₂ and the opened DC CB at B₂₃. For this reason, observed from the local end at B₁₂, a period of wave-oscillation will be detected.

Define the cycle of the oscillation wave T' as the time interval when the local protection at B₁₂ successively detects a forward wave-front and a reverse wave-front. For illustrative purposes, the duration of 'A-B-C' shown in Fig. 1(c) is the oscillation wave T' cycle when an external fault occurs. The cycle T' and the oscillation frequency f' can be written as:

$$\begin{cases} T' = 4 \frac{l}{v_1} \\ f' = \frac{1}{T'} \end{cases} \quad (5)$$

From Equation (5), when an external fault occurs at the head of the adjacent line, the oscillation frequency f' is only related to the total length of the local line l .

Internal dead-zone faults

Under the internal fault condition, the transient process of traveling wave propagation is shown in Fig. 1(b), where x is the local-line length percentage of the distance from the fault point F2 to remote-end protection at B₂₁. The reverse wave V_{lwb} and the forward wave V_{lwf} are generated after the occurrence of the internal dead-zone fault at F2, and the reverse wave V_{lwb} propagates to the local-end protection at B₁₂. Let the moment when the main wave arrives at B₁₂ be t_{in}^1 . The forward traveling wave V_{lwf} propagates forward along the line to the remote-end protection at B₂₁. As the fault is very near to B₂₁, it is regarded as internal by the protection equipped at B₂₁, since this is a near-end fault in the view of the protection element at B₂₁. Therefore, this protection element outputs a trip signal to the DC CB B₂₁, and the breaker will open after a delay of T_0+T_b . From this moment on, a second wave V_{2wb} caused by the opening of DC CB B₂₁ will reflex and refract between the end of the DC line and the fault point repeatedly.

The refraction wave $\Gamma_{11}V_{2wb}$ propagates in a reverse direction and arrives at local-end protection at B₁₂. Let the moment when the second wave arrives first time at B₁₂ be t_{in}^2 . The reflection wave $\Lambda_{11}V_{2wb}$ propagates in the forward direction and arrives at B₂₁. Due to the opening of B₂₁, this wave is totally reflected, and this process will repeat several times until the complete attenuation of the wave. Under this condition, the time difference Δt_{in} can be deduced by:

$$\begin{cases} t_{in}^1 = \frac{l-xl}{v_1} \\ t_{in}^2 = \frac{xl}{v_1} + T_0 + T_b + \frac{l}{v_1} \\ \Delta t_{in} = t_{in}^2 - t_{in}^1 = T_0 + T_b + \frac{2xl}{v_1} \end{cases} \quad (6)$$

As indicated in Equation (6), the time difference Δt_{in} is related to x and l under the internal-fault condition. In comparison with that in the external-fault condition, it is evident that

$\Delta t_{in} \geq \Delta t_{out}$. According to the process of traveling wave propagation, the cycle T and oscillation frequency f can be obtained as follows:

$$\begin{cases} T = 4 \frac{xl}{v_1} \\ f = \frac{1}{T} \end{cases} \quad (7)$$

As noted in Equation (7), when an internal fault occurs in the dead-zone, the oscillation frequency f is related to the total length of the local line l and the fault location x . Note that the length of the line l is much longer than the length of xl . As a result, a larger level of wave-oscillation can be observed in the internal fault scenario, which can explain the difference between Fig. 1(c) and Fig. 1(d).

3) Sampling frequency and the absolute dead zone

According to the Nyquist sampling theorem, the sampling frequency γ should be at least twice the signal frequency to avoid signal aliasing. In terms of engineering practice, for a specific sampling frequency, there should be a theoretical maximum detectable frequency f_m , which is given by:

$$\gamma > 2f_m \quad (8)$$

From Equation (7), it is evident that oscillation frequency f is interrelated with the distance of xl . Due to the limitation of the sampling frequency, once the fault is too close to the local-end protection element, the oscillation frequency f will be no longer distinguishable. The relationship between f and this zone, which is denoted by ε , can be obtained by substituting Equation (7) into (8):

$$\varepsilon = \frac{v_1}{2\gamma} \quad (9)$$

According to the above, the relationship between the two is shown in Fig. 2. Theoretically, the absolute dead zone can be reduced infinitely by using very high sampling rates. According to Equation (9), if the sampling frequency is 200 kHz, the length of the absolute dead zone ε should be 0.754 km, theoretically.

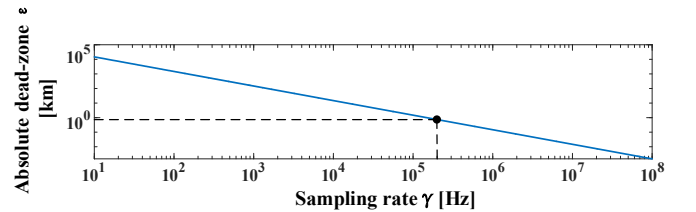


Fig. 2 The sampling rate and absolute dead-zone

III. Methodology

A. Introduction to wavelet time-entropy

Assume that $x(t)$ is a continuous signal at the time domain and $\psi(t)$ is the basis of wavelet functions. The discrete wavelet transform (DWT) of the continuous signal $x(t)$ is given by:

$$DWT(2^h, 2^h s) = \frac{1}{2^{h/2}} \int_{-\infty}^{\infty} x(t) \Psi\left(\frac{t-2^h s}{2^h}\right) dt \quad (10)$$

Among them, $DWT(2^h, 2^h s)$ is the wavelet coefficient, and $\psi(t)$ use the dilation 2^h and translation $2^h s$ parameters. h

represents the number of scales of the wavelet decomposition. DWT is a method to calculate the similarity of $x(t)$ and $\psi(t)$. By repeatedly stretching and sliding the wavelet, the frequency and time information of the signal is obtained.

To analyze a specific signal, DWT is equal to recursively filtering the signal with a high-pass and a low-pass filter-pair. Details are produced by high-pass filters, and approximations are produced by low-pass filters. The bandwidth of these two filters is equal. After each circle of decomposition, the sampling frequency is reduced by half. In this process, $D_h(t)$ represents the component of the transient signal $x(t)$ at each scale (frequency band) [21], which is given by:

$$D_h(t) = 2^{-\frac{h}{2}} \sum_{-\infty}^{\infty} DWT(2^h, 2^h s) \Psi(2^{-h} t - s) \quad (11)$$

For illustrative purposes, the process of detail coefficient construction is illustrated in Fig. 3.

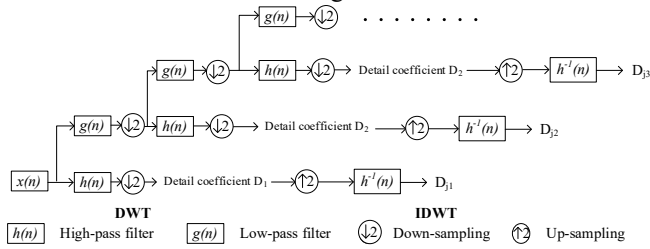


Fig. 3 DW transformation and construction

According to the Nyquist sampling theorem and DWT frequency band segmentation, the corresponding frequency band of the DWT construction signal at scale- h is $[2^{-(h+1)}\gamma, 2^{-h}\gamma]$. To analyze a real-time varying signal, define a sliding time window given by $D_h(t)$ in Equation (12), where ω is the window length, and σ is the sliding step length ($m=1, 2, 3, \dots$).

$$W(m; \omega; \sigma) = \{D_h(t), m\sigma \leq t \leq \omega + m\sigma\} \quad (12)$$

Let S_0 and S_L be the maximum and minimum bounds of the signal in the sliding window:

$$\begin{cases} S_0 = \min[W(m, \omega, \sigma)] \\ S_L = \max[W(m, \omega, \sigma)] \end{cases} \quad (13)$$

Divide the sliding window into L intervals:

$$\begin{cases} W(m; \omega; \sigma) = \bigcup_{l=1}^L Z_l, & Z_1 \cap Z_2 \cap \dots \cap Z_L = \emptyset \\ Z_l = [S_{l-1}, S_l]; & l = 1, 2, \dots, L; \quad S_0 < S_1 < S_2 \dots < S_L \end{cases} \quad (14)$$

In Equation (15), $p_z^h(Z_l)$ is the probability that the points of the signal in the h -th layer, m -th time window falling in the interval of Z_l . Then, the WTE $H_{WTE}^h(m)$ is defined as follows:

$$H_{WTE}^h(m) = -\sum_{l=1}^L p_z^h(Z_l) \log_n(p_z^h(Z_l)) \quad (15)$$

where $-\log_n(p_z^h(Z_l))$ denotes the self-information of the signal $D_h(t)$ in the time window, and the mathematical expectation of such self-information can express the included information of a signal. The more significant the fluctuation of the signal is, the larger the information the signal carries.

According to Equation (15), WTE is finally calculated to quantify the extent of fluctuation of the signal component

$D_h(t)$ after wavelet reconstruction of the signal $x(t)$, which can represent the level of oscillation in the observed frequency bands. This helps reveal the inherent characteristics of fault components.

Due to the discrete sampling process of the signal, there must be discontinuous sampling signals, which generate spectrum leakage caused by the singularity. Assuming that the sampling frequency is 200 kHz, we will have six high-frequency bands, and the corresponding detail coefficients are d1~d6, covering 1.56 kHz-100 kHz. To avoid the effect of spectrum leakage, a6 and d1~d3 coefficients are not used. Coefficients d4~d6 are taken to reconstruct the waveform.

To ensure reliability, $H_{WTE}^4(t)$, $H_{WTE}^5(t)$, and $H_{WTE}^6(t)$ are utilized to determine the type of faults according to the principle of 2-of-3.

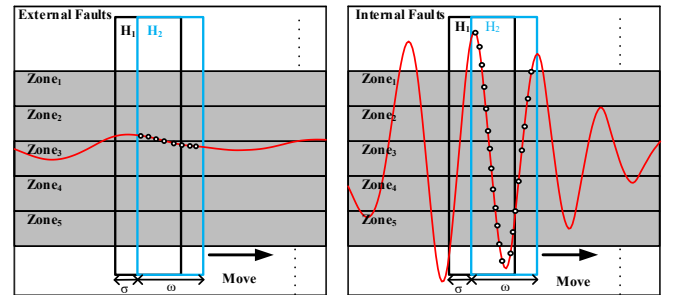
B. Wavelet time-entropy under different types of fault-conditions

When an external fault occurs, the second traveling wave caused by the opening of the adjacent line's DC CB comes through the converter station and reflects between the head of a local DC line and the head of the adjacent line. However, the oscillation frequency is too low compared with the internal fault condition. For illustrative purposes, the situation of the traveling-wave waveform in this scenario is shown in Fig. 4(a). The maximum value of the entropy caused by the second traveling wave is:

$$\begin{cases} p_z = n_z / N & (0 \leq p_z \leq 1) \\ f(p_z) = p_z \log_n p_z \\ H_{WTE} = -\sum_{z=1}^n f(p_z) \end{cases} \quad (16)$$

where p_z is the probability of the sampling point falling in each zone, denoted as n_z/N . N is the total number of sampling points in the sliding window, and n_z is the number of that in a specific zone. Thus, when an external fault occurs, the maximum of the entropy H_{WTE} is given by:

$$H_{WTE}^{\max} = 2e^{-1} \log_n e^{-1} \quad (17)$$



(a) External fault condition (b) Internal fault condition
Fig. 4 $D_h(t)$ calculation under different fault conditions

Under the internal dead-zone fault condition, the local-end protection can detect a period of wave-oscillation. Theoretically, if a great disturbance appears in a signal, it means that the entropy has a considerable increase. The situation is shown in Fig. 4(b) for illustrative purposes in this scenario. Once the fluctuation of the waveform becomes more significant than that under the external fault condition, the entropy

value will exceed the maximum value $2e^{-1}\log_n e^{-1}$, according to the above analysis. By this means, faults are classified into external and internal.

C. The proposed WTE-based criterion considering operations of DC CB

The requirement for the speed of internal-fault-isolation for the MMC-MTDC is just several milliseconds, and the typical value is 5 ms. For this reason, the protection has to consider the DC CB operation time and its process. The typical topology of the DC CB is shown in Fig. 5.

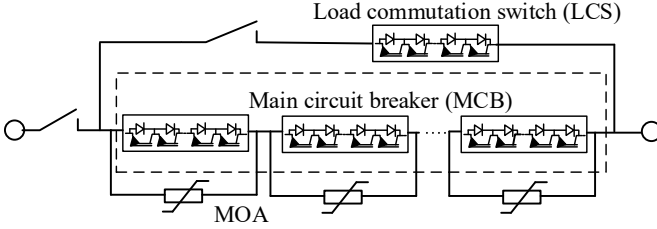


Fig. 5 The topology of DC CB

Once the local-end protection detects the arrival of the main traveling wave caused by the occurrence of the fault, firstly, the fault will be determined if it is an internal one according to the decision of local-measurement-based protection elements. In some cases where the primary protection fails to operate due to the lack of sensitivity, the proposed criterion starts to double-check if this fault is within the dead-zone of the remote end. In case of communication anomalies, only local measurements are accessible. According to the analysis in Section II, the arrival time of the second wave is at least T_0+T_b . Thus, taking the arrival time of the main traveling wave as the starting point of the proposed criterion, it is very sure that the arrival of the second wave can be captured after a delay of T_0+T_b . From this moment on, whether the fault is internal but in the remote-end dead-zone is further determined. The detailed procedure is shown in Fig. 6.

The primary protection cooperating with the proposed criterion is in Reference [22]. This is also a local-measurement-based non-unit protection element based on the arrival time difference of the aerial- and zero-mode traveling waves ($\tau=|t_1-t_0|$), which is very sensitive for local-end faults, and it can cover at least 85% of the full length of a DC line but not sensitive enough against remote-end faults. In this paper, the mathematical expression of the above primary protection is modified to:

$$\begin{cases} 0 \leq \tau < \tau_1 & \text{(a) Internal fault} \\ \tau_1 \leq \tau < \tau_2 & \text{(b) Unidentified fault} \\ \tau_2 \leq \tau \leq \tau_3 & \text{(c) External fault} \end{cases} \quad (18)$$

According to Equation (18), situations (a), (b) and (c) are determined. Among them, (a) represents the internal fault that needs to trip the DC CB immediately without a further determination by the proposed criterion, (b) represents the

unidentified fault that may be located in the remote-end dead-zone of the local line or the terminal of the adjacent line that requires further determination, and (c) represents the external fault that does not need to trip the local DC CB. Evidently, scenario (b) is the main focus of this paper, which is further determined according to the following.

- 1) Under the normal operating condition, the proposed criterion works in cooperating with the primary protection in real-time, and local measurements are monitored. When a fault occurs, fault scenarios are pre-determination according to Equation (18).
- 2) In the case of scenario (a), the primary protection determines this fault as internal. DC CB receives the tripping signal, transfer the current from the main branch to the current-transferring branch, and switch in the energy consumption Metal Oxide Arrester (MOA) to interrupt the faulted current. In the case of scenario (c), the primary protection determines this fault as external and then returns to the normal status in Step 1). In the case of scenario (b), the DC CB will transfer the current from the main branch to the current-transferring branch but will not switch in the MOA immediately. Whether it is necessary to switch in the MOA depends on the following steps.
- 3) Taking the arrival time of the main traveling-wave as the starting point, the proposed criterion begins to work after a delay of T_0+T_b , because (1) the arrival of the second wave and the happening of oscillations will not be earlier than this moment; (2) the current-transferring can be finished within this duration. When the proposed criterion works, a time window of ω is opened to truncate the local aerial-mode traveling wave.
- 4) The window will slide for a total of $(T_m-(T_b+T_0))$ milliseconds, where T_m is the critical fault-clearing time of the H-MMC. In each sliding step, the waveform is analyzed, and the WTE is determined in real-time, based on which H_{WTE}^4 , H_{WTE}^5 , and H_{WTE}^6 are calculated.
- 5) At the end of the sliding procedure, the unidentified fault will be classified according to the feature of the calculated WTE. If two or more out of three calculated WTEs exceed the threshold, the fault is internal. The local-end DC CB will switch in the MOA immediately in this scenario, interrupting the fault current. Otherwise, the current will be released from the current-transferring branch to the DC line, indicating that the fault is external that does not need the operating of the DC CB.

For an illustrative purpose, the cases of external fault scenario, internal fault scenario, an unidentified fault being determined as external, and an unidentified fault being determined as internal are shown in Figs. 7(a), (b), (c), and (d), respectively, including the time-sequence, the operating logic of the proposed criterion, and the operating logic of the DC CB.

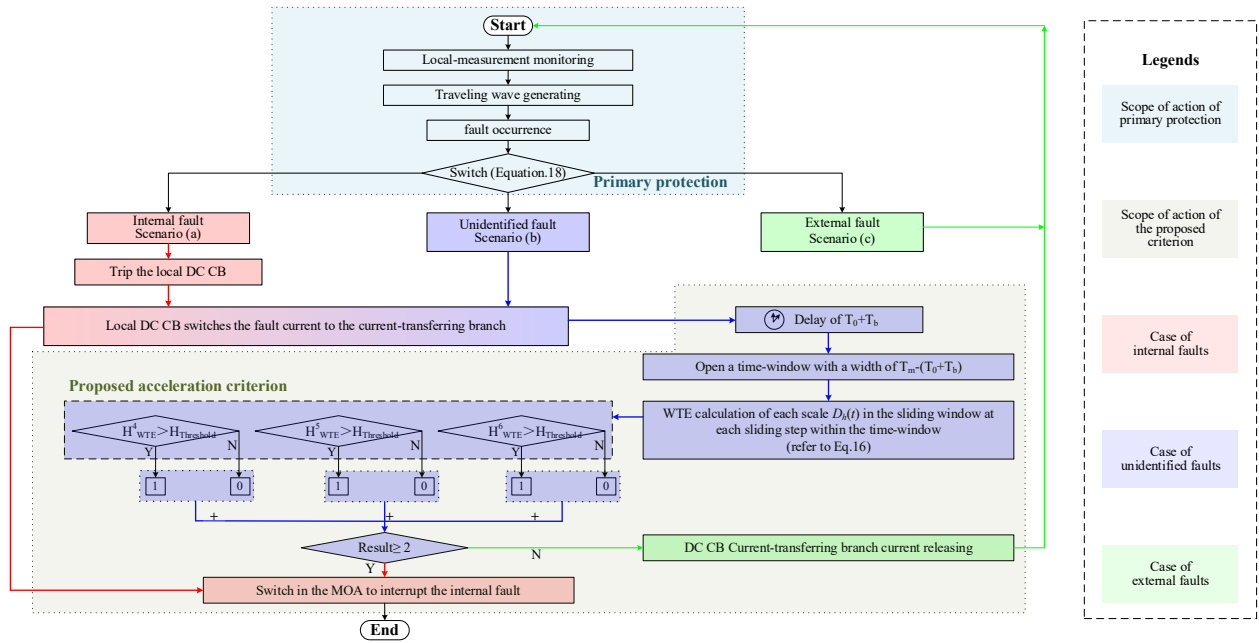
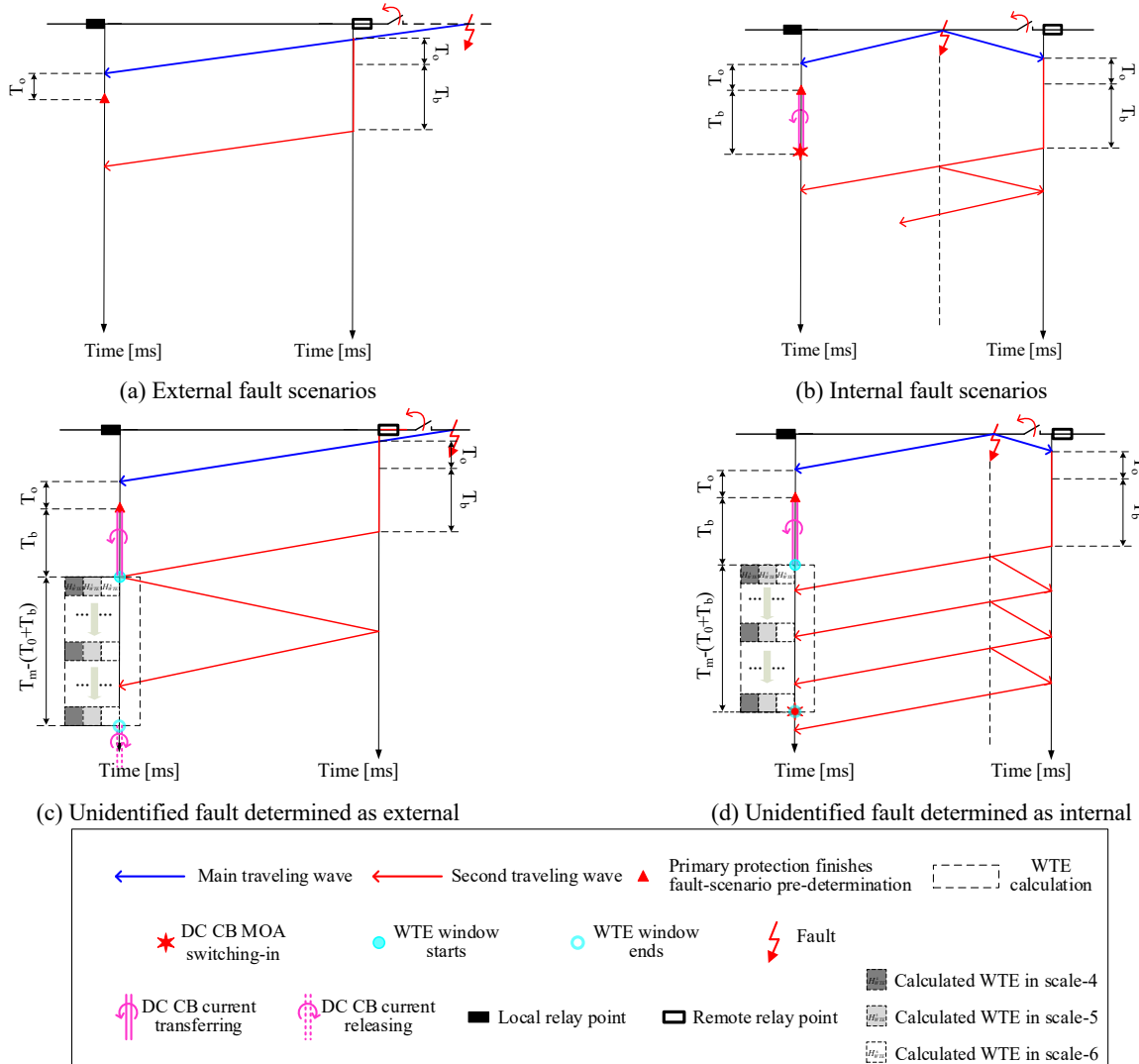


Fig. 6 The flowchart of the proposed criterion



(e) The legends

Fig. 7 A time-sequence diagram for the determination of fault scenarios

IV. Simulation studies

In this section, simulation studies are conducted to assess the performance of the proposed criterion. To this aim, an MMC-MTDC system based on the Zhangbei four-terminal DC grid structure is established on the PSCAD/EMTDC platform. The established model is shown in Fig. 8, where the parameters for each line and model of overhead lines are given in Appendix Table A1 and Fig. A1. The frequency-dependent characteristics of each DC line is calculated according to Table A1 and Fig. A1(a) and shown in Fig. A1(b).

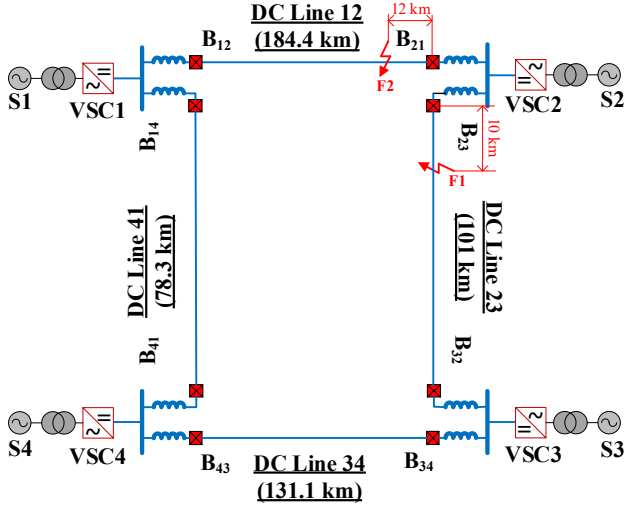


Fig. 8 The topology of established MMC-MTDC

Set the sampling frequency of the simulation model to 200 kHz. Based on the DC line model, the aerial-mode traveling wave velocity v_1 is 2.97×10^8 m/s. Typically, T_b and T_0 are set to 2.0 ms and 0.5 ms, respectively. To have competitive results, T_m is set as 5 ms for MMC-MTDC, which means the longest fault-endurance time for the continuous operation of the MMC converter is merely 5 ms. Also, the width and the sliding step of the sliding window affect the performance of the proposed criterion. For this reason, at least one period of the wave-oscillating should be captured in each sliding window. To cover a certain level of error, the width of the sliding windows should be wider than the maximum period of the oscillation wave T_{om} . Besides, the sliding step should be set as short as possible to enhance the time resolution.

Taking DC line 12 as an example, according to Equation (7), the maximum period of the oscillation wave T_{om} is 0.37 ms. Considering a certain level of time-margin, the width of the sliding windows ω is set to 0.4 ms. Furthermore, the sliding step is set to 5 μ s, equal to the given sampling rate. The setting of the parameters in this paper is listed in Table 1.

Table 1 Parameter settings

Line	Length [km]	ω [ms]	σ [μ s]	S_0	S_L
DC line 12	184.4	0.40	5	-120	120
DC line 23	101	0.25	5	-120	120
DC line 34	131.1	0.30	5	-120	120
DC line 41	78.3	0.20	5	-120	120

In Equation (16), the value of base n in the mathematical expression of WTE has no impact on the relative comparison

of entropy under different fault situations. Thus, n might as well be set to 2. By this means, the unit of entropy is 'bit'. According to Equations (16) and (17), this threshold is set to 1.6 bit, considering a certain level of margin to improve the security of the protection.

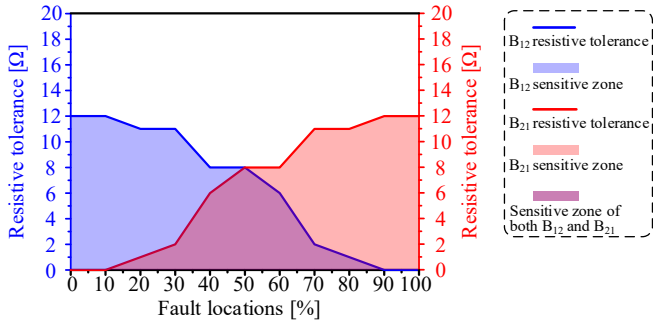
Before the simulation study, the performance of the primary protection and the necessity of the proposed protection is analyzed. Conventionally, traveling-wave-based protection elements work as the primary protection for MMC-MTDC. Taking the traveling wave protection, also known as the so-called wave-front protection for DC line-to-ground fault (WFPDL), as an example, the primary protection criterion is as follows:

$$\begin{cases} \left| \int_t^{t+t_d} [\Delta u_1(t) - Z_1 \times \Delta i_1(t)] dt \right| > S_{1_set} \\ \left| \int_t^{t+t_d} [\Delta u_0(t) - Z_0 \times \Delta i_0(t)] dt \right| > S_{0_set} \\ |\Delta u_0(t) - Z_0 \times \Delta i_0(t)| > \Delta S_{0_set} \end{cases} \quad (19)$$

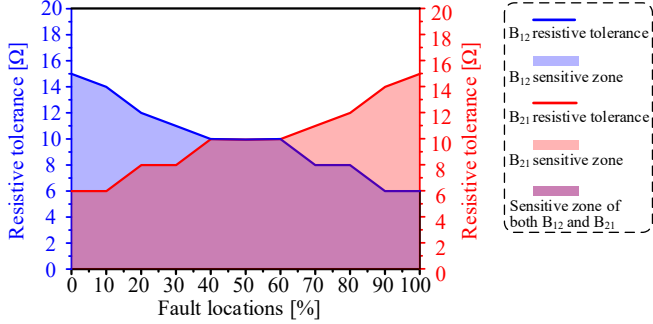
where $\Delta u_1(t)$ is the superimposed component of the aerial-mode voltage, $\Delta i_1(t)$ is the superimposed component of the aerial-mode current, $\Delta u_0(t)$ is the superimposed component of the zero-mode voltage, and $\Delta i_0(t)$ is the superimposed component of the zero-mode current. t_d is the time window of the WFPDL (set to 0.5 ms in an MMC-MTDC). S_{1_set} , S_{0_set} , and ΔS_{0_set} are the setting values of the aerial-mode backward traveling wave, the zero-mode backward traveling wave, and the differential of the zero-mode backward traveling wave, respectively. The setting principle is to avoid the fault that occurs at the backside of the CLR equipped at the end of the DC line.

In addition, the new primary protection elements based on the time-difference of wave-arrival work well. Taking the primary protection in Reference [22], the basis of the protection element is the detection of the arrival difference between the fault-induced zero-mode traveling wave and the aerial-mode traveling wave. For scenario (a), when the result is in Equation (18), it will trip the fault immediately. In the case of scenario (b) or (c), the protection will return without further determination.

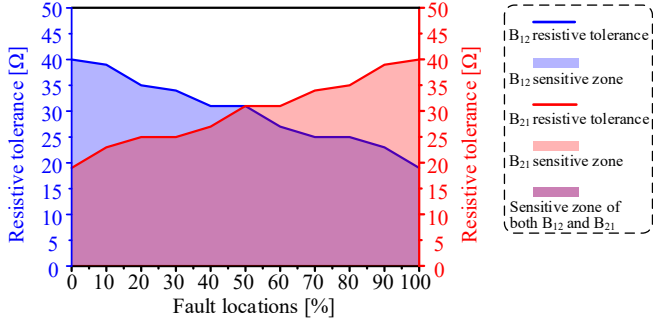
The performance of the protection elements B_{12} and B_{21} is studied when the CLR is set to 100 mH, 150 mH, 200 mH, and the performance the above two types of protection elements is shown in Fig. 9 and Fig. 10. The setting value of the WFPDL is listed in Table A2. It can be seen that both types of protection elements are sensitive to the faults near the local end. For the WFPDL, the resistive tolerance against near-end fault can be 12 Ω -40 Ω , whereas the resistive tolerance declines sharply against remote-end fault. As a result, for the blue area in Figs. 9(a), (b), and (c), B_{12} can trip the fault, but B_{21} is not sensitive enough; in contrast, for the red area, it is the sensitive zone of B_{21} but the remote-end dead-zone for B_{12} . Using the proposed protection element in Reference [22], the sensitivity against near-end faults is enhanced. However, under the remote-end fault condition, the protection element cannot trip even a bolted grounding fault. When there are communication anomalies, only the local-end protection element can trip the fault, which is the problem aimed to be solved.



(a) CLR value 100 mH



(b) CLR value 150 mH



(c) CLR value 200 mH

Fig. 9 The performance of the WFPDL

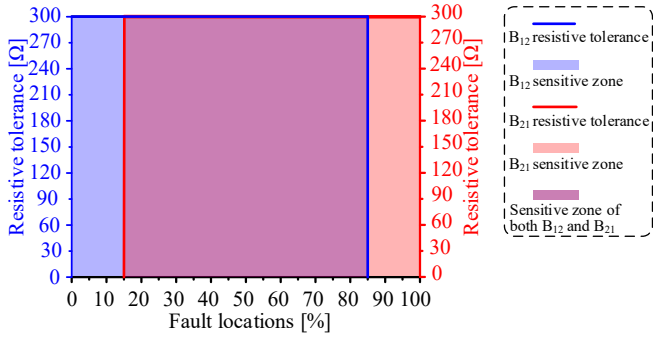


Fig. 10 The performance of the protection in Reference [22]

A. Security test

First, to assess the security of the proposed criterion, a pole-to-ground external fault is applied at F1 when $t=0$ ms, which is 10 km from the converter station of the adjacent DC line. The above fault-inception induces the main traveling wave. After a time-delay $T_0+T_b=2.5$ ms, DC CB B₂₃ opens as the local-end protection trips the fault F1, which generates the second traveling wave. For illustrative purposes, the time-sequence for the above fault-induced transient is shown in Fig. 11.

(i). First, the main traveling wave arrives at DC line 23 local-end protection, where the DC CB B₂₃ received the tripping

signal. (ii). Then, the main traveling wave arrives at protection B₁₂, where the DC CB B₁₂ starts current-transferring. (iii). After inherent delay $T_b=2$ ms and main protection time window $T_0=0.5$ s, the DC CB B₂₃ opens for tripping the fault F1, triggering the second wave presented as the red line. (iv). The DC CB B₁₂ completes the current transferring. (v). The second wave arrives at B₁₂. (vi). The proposed criterion starts to work while the time window starts and slides through the time. (vii). The local-end protection closes the time window. From the main-wave arrival to the end of the WTE time window, the total time spent on the determination of the fault is $T_m=5$ ms, which is the typical fault-endurance time for an MMC-MTDC. It means a time margin of 2.5 ms is left for the proposed criterion to distinguish whether it is an internal or external fault.

In this scenario, the local-end protection at B₁₂ detects the arrival of the second wave at $t=3.15$ ms. Then, the proposed criterion starts to work from $t=3.15$ ms using a sliding time window with a width of 0.4 ms. As shown in Fig. 12, the sliding time window moves with a sliding step of $\sigma=5$ μ s from 3.15 ms to 5.65 ms, which lasts for 2.5 ms. In each step, the WTE of each scale is calculated, as shown in Fig. 13. The obtained waveform is a relatively smooth one.

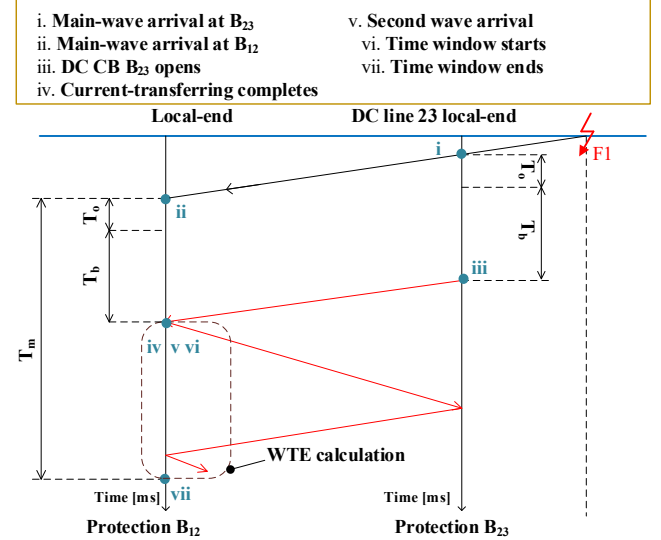


Fig. 11 Time-sequence of external fault occurrence

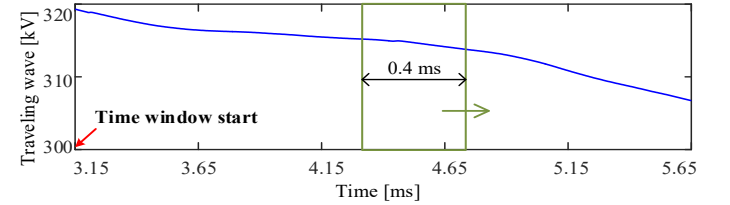
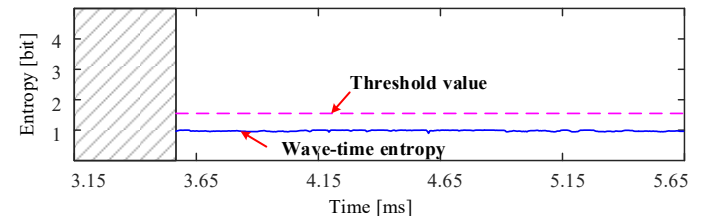
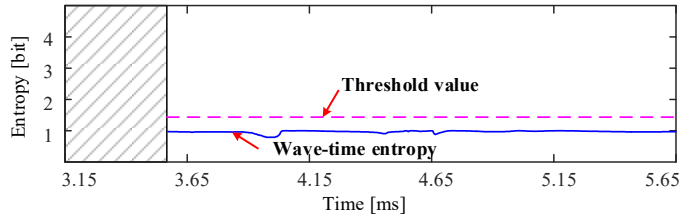


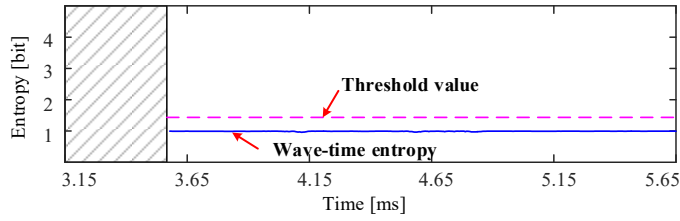
Fig. 12 Aerial-mode traveling wave at under external fault F1



(a) 4th scale wave-time entropy under external fault F1



(b) 5th scale wave-time entropy under external fault F1



(c) 6th scale wave-time entropy under external fault F1

Fig. 13 The performance of WTE against external fault

As illustrated, there is a 0.4-ms shaded area because the first WTE value is only accessible after 0.4 ms from the starting of the sliding window. The WTE value in each scale inside the time window is always lower than the threshold (1.6 bit), indicating a very low variation for the observed waveform. For this reason, the local-end protection at B₁₂ determines this fault as an external one. As a result, the DC CB B₁₂ recovers to the normal operating condition by releasing the current from the transfer-loop to the DC line at $t=5.65$ ms. Thus, the proposed WTE has high security under this condition.

B. Performance under internal fault condition

To assess the performance of the proposed criterion under the internal fault condition, different types of faults at F2 are set, which are 12 km far from the local end of B₁₂. The time sequence for the above process is shown in Fig. 14.

(i). First, the main traveling wave caused by the fault at F2 arrives at remote-end protection, and the DC CB B₂₁ receives the tripping signal. (ii). Then, the main traveling wave arrives at the local-end protection, where the DC CB B₁₂ starts current-transferring. (iii). For B₂₁, after the arrival of the main wave, the DC CB B₂₁ opens and triggers the second wave presented as the red lines. (iv). The DC CB B₁₂ completes the current transferring. (v). The second wave arrives at B₁₂. (vi). The proposed criterion starts to work while the time window starts and slides through the time. (vii). The local-end protection closes the time window.

When the incepted fault is a pole-to-ground fault at $t=0$ ms, the above fault-inception induces the main traveling wave. After a time delay of 2.5 ms, DC CB B₂₁ opens as the local-end protection and trips the fault, which generates the second traveling wave. As shown in Fig. 15, the local-end protection at B₁₂ detects the arrival of traveling-wave at $t=3.16$ ms, and the proposed criterion starts to work at $t=3.08$ ms using a sliding time window with a width of 0.4 ms. As shown in Fig. 16, the values of WTE in the 4th, 5th, 6th scales are all higher than the threshold value (1.6 bit), indicating that this is an internal fault according to the principle of 2-of-3. In this scenario, the MOA of the local DC CB at B₁₂ is switched in at $t=3.58$ ms.

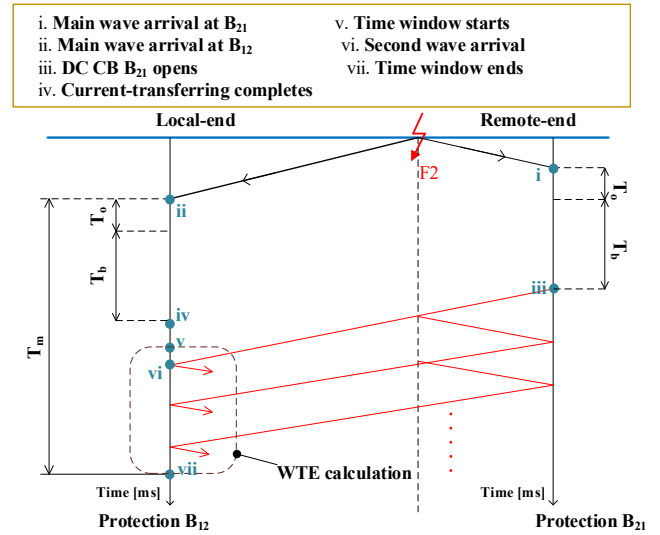


Fig. 14 Time-sequence of internal fault occurrence

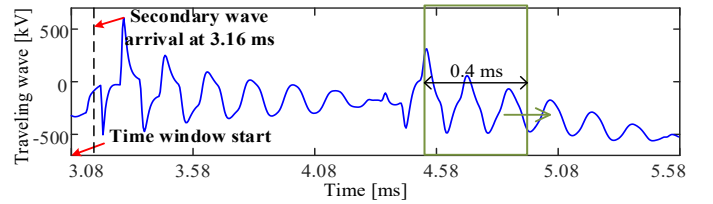
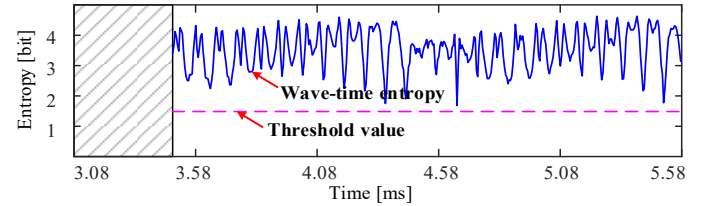
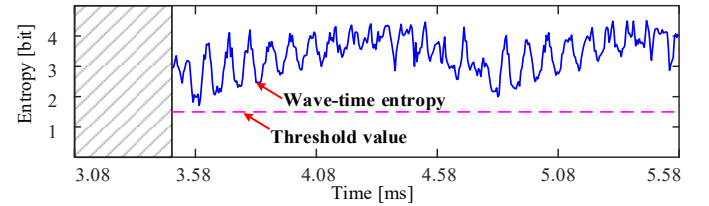


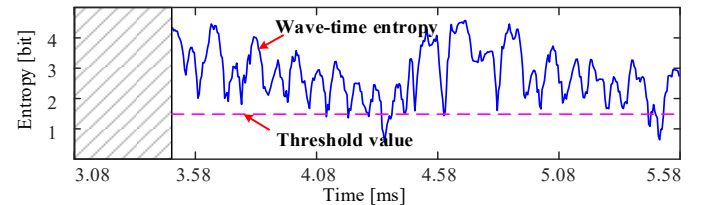
Fig. 15 Aerial-mode traveling wave under internal fault F2



(a) 4th scale wave-time entropy under internal fault F2



(b) 5th scale wave-time entropy under internal fault F2



(c) 6th scale wave-time entropy under internal fault F2

Fig. 16 WTE against internal p-g fault (0 Ω)

In actual engineering applications, DC line faults are often accompanied by fault resistances. Hence, it is necessary to assess the performance of the proposed criterion under high-resistance fault conditions. Keeping other conditions unchanged, the fault resistance is changed to 300 Ω , which is the upper limit of the fault resistance that should be considered for 500-

kV systems. As the fault location is still F2, the same time sequence in Fig. 14 still works under this condition. Similarly, the observed traveling wave is shown in Fig. 17, and the corresponding WTE results are shown in Fig. 18.

As indicated, the value of WTE declines sharply. However, the local-end protection at B₁₂ can still trip the local DC CB since the calculated WTEs in the 3 scales are higher than the threshold. Similarly, the MOA of the local DC CB at B₁₂ is switched in at t=5.58 ms due to the detection of an internal fault.

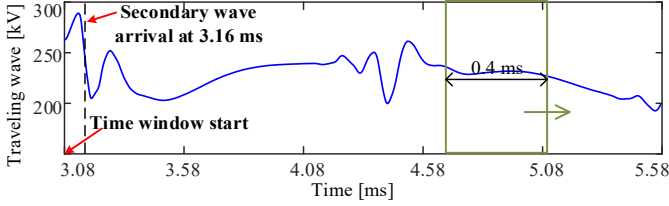


Fig. 17 Aerial-mode traveling wave under internal fault F2 (300 Ω)

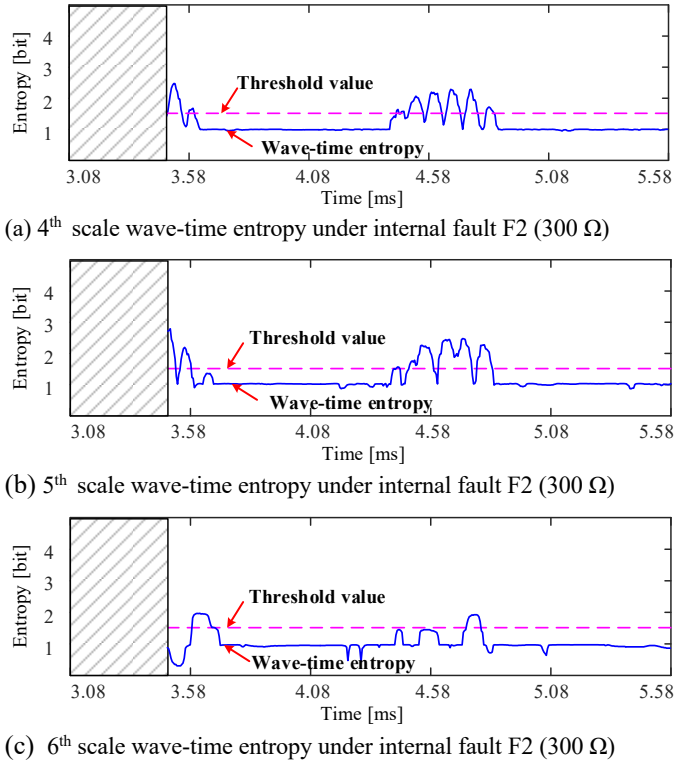


Fig. 18 WTE against internal p-g fault (300 Ω)

C. Performance assessment

To have a total view of the proposed criterion's resistive-tolerance, repeated tests are conducted with different fault locations and fault-resistances in this section. Whether the local-end protection can trip the dead-zone fault is investigated and recorded. The results are shown in Fig. 19. Taking the local-end protection at B₁₂ as an example, the proposed protection has the following features:

- 1) The local-end protection at B₁₂ is unable to detect the fault at the location from 156.8 km (85%) to the end of DC line 12 (100%). After using the proposed criterion, the fault occurring from the local-end (0%) to 183.9 km (99.56%) can all be detected effectively with relatively high resistive tolerance. Thus, the protective range of the local-end protection at B₁₂ enhances from 0%-85% to 0%-99.56%.

- 2) When the fault occurs at 99.56% to 100% range of the DC line 12, the oscillation frequency of the traveling wave received by the local-end protection at B₁₂ is extremely high due to the fault point being too close to the opposite bus, which already exceeds the upper limit of frequency that the proposed criterion can reach. Under the realistic condition that the sampling rate cannot be increased unlimitedly, though greatly decreased, a short dead-zone still exists in the proposed protection. For the four DC lines mentioned above, the length range of the dead-zone is 0.43%, 0.99%, 0.76%, 1.14% respectively.
- 3) The above result is under the condition that the utilized sampling rate is 200 kHz. According to the Nyquist-Shannon sampling theorem, the signal with a frequency greater than 100 kHz cannot be captured. If the sampling rate can increase in the future practical engineering application, the performance of the proposed protection can be further improved.

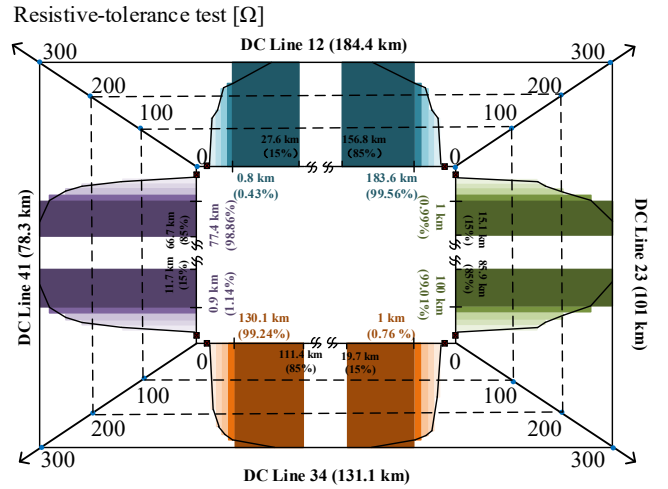


Fig. 19 Performance of WTE fault resistance test at MMC-MTDC

V. Conclusion

To improve the sensitivity of the local-measurement-based protection element against remote-end faults, a wavelet-time-entropy-based acceleration criterion is proposed in this paper. A sliding time window is set to calculate the WTE value after the arrival of the second traveling wave, which can characterize the 'chaos' level of the observed wave signal. According to the results, the following conclusions can be achieved:

- 1) With the help of the proposed acceleration criterion, a significant decrease in the length of dead zones (approximately 15%) can be achieved. For the four DC lines with lengths of 184.4 km, 101 km, 131.1 km, and 78.3 km, the remaining dead zones are 0.43%, 0.99%, 0.76%, and 1.14%, which can be further reduced by increasing the sampling frequency.
- 2) In most cases, the resistive tolerance of the dead-zone grounding faults can be as high as 300 Ω. The proposed criterion performs less satisfactorily in cases where the fault is very close to the remote-end DC bus bar.
- 3) The proposed criterion has sufficient time to trip the local-end DC CB before the blocking of the MMC converter because once the fault is an unidentified one, the local-end DC

CB will execute the current-transferring procedure immediately before the final determination of the fault type, in case that the fault is internal according to the calculation of WTE. Thus, high security of the operation of the MMC is ensured.

Acknowledgments

This work was supported by the National Natural Science Foundation of China under grant number 51907069.

CRedit authorship contribution statement

N. Tong: Conceptualization, Methodology, Software, Writing- Original draft preparation, Funding acquisition; Z. Tang: Methodology, Data curation, Writing- Reviewing and Editing, Writing- Original draft preparation; C. S. Lai: Conceptualization, Writing- Reviewing and Editing, Supervision; X. Li: Writing- Reviewing and Editing, Visualization; A. Vaccaro: Conceptualization, Writing- Reviewing and Editing; L. L. Lai: Conceptualization, Writing- Reviewing and Editing, Supervision, Funding acquisition, Resources.

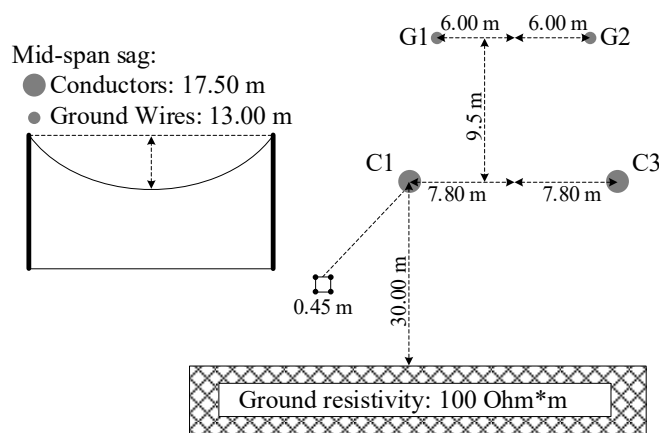
Appendix

Table. A1 The DC line parameters

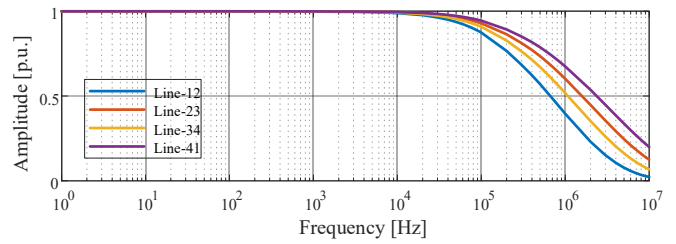
System parameters	Value
Rated DC voltage [kV]	±500
Number of sub-modules	200
CLR [mH]	150
Arm reactance [mH]	Station-1: 61.7; Station-2: 61.7; Station-3: 30.8; Station-4: 30.8
Capacitance of sub-module [μF]	Station-1: 16292; Station-2: 16292; Station-3: 32584; Station-4: 32584

Table. A2 The setting of the WFPDL

FCL reactor [mH]	S_{1_set} [kV]	S_{0_set} [kV]	ΔS_{0_set} [kV/ms]
100	253.4	322.6	4.2
150	199.7	260.5	3.1
200	161.1	216.1	2.4



(a) features of the overhead DC line



(b) frequency-dependent characteristics of the overhead DC line

Fig. A1 The model of DC transmission line

References:

- [1].Sun, K., Xiao, H., Pan, J., et al., A station-hybrid HVDC system structure and control strategies for cross-seam power transmission. *IEEE Transactions on Power Systems*, 2020. 36(1): pp. 379-388.
- [2].Lai, C.S., Jia, Y., Lai, L., et al., A comprehensive review on large-scale photovoltaic system with applications of electrical energy storage. *Renewable and Sustainable Energy Reviews*, 2017. 78: p. 439-451.
- [3].Ruiwen, H., D. Jianhua., L.L. Lai., Reliability evaluation of communication-constrained protection systems using stochastic-flow network models. *IEEE Transactions on Smart Grid*, 2017. 9(3): pp. 2371-2381.
- [4].Sun, K., Li, K., Lee, W., et al., VSC-MTDC system integrating offshore wind farms based optimal distribution method for financial improvement on wind producers. *IEEE Transactions on Industry Applications*, 2019. 55(3): pp. 2232-2240.
- [5].Sun, K., Li, K., Pan, J., et al., Frequency response reserves sharing across asynchronous grids through MTDC system. *IET Generation, Transmission & Distribution*, 2019. 13(21): pp. 4952-4959.
- [6].Suonan, J., Gao, S., Song, G., et al., A novel fault-location method for HVDC transmission lines. *IEEE Transactions on Power Delivery*, 2009. 25(2): pp. 1203-1209.
- [7].Bin, L.L., He, J., Tian, J., et al., DC fault analysis for modular multilevel converter-based system. *Journal of Modern Power Systems and Clean Energy*, 2017. 5(2): pp. 275-282.
- [8].Le Blond, S., Bertho Jr, R., Coury, D.V., et al., Design of protection schemes for multi-terminal HVDC systems. *Renewable and Sustainable Energy Reviews*, 2016. 56: pp. 965-974.
- [9].Eissa, M.M., Protection techniques with renewable resources and smart grids—A survey. *Renewable and Sustainable Energy Reviews*, 2015. 52: pp. 1645-1667.
- [10].Sabug Jr, L., Musa, A., Costa, F., et al., Real-time boundary wavelet transform-based DC fault protection system for MTDC grids. *International Journal of Electrical Power & Energy Systems*, 2020. 115: 105475
- [11].Nadeem, M.H., Zheng, X., Tai, N., et al., Non-communication based protection scheme using transient harmonics for multi-terminal HVDC networks. *International Journal of Electrical Power & Energy Systems*, 2021. 127: 106636
- [12].Chu, X., Song, G., Liang, J., Analytical method of fault characteristic and non-unit protection for HVDC transmission lines. *CSEE Journal of Power and Energy Systems*, 2016. 2(4): p. 37-43.
- [13].Ara, R., Khan, U.A., Bhatti, A.I., et al., A reliable protection scheme for fast DC fault clearance in a VSC-based meshed MTDC grid. *IEEE Access*, 2020. 8: pp. 88188-88199.
- [14].Duan, J., Li, H., Lei, Y., et al., A novel non-unit transient based boundary protection for HVDC transmission lines using synchroqueezing wavelet transform. *International Journal of Electrical Power & Energy Systems*, 2020. 115: 105478.
- [15].Huang, Q., Zhou, G., Wei, X., et al., A non-unit line protection scheme for MMC-based multi-terminal HVDC grid. *International*

- Journal of Electrical Power & Energy Systems*, 2019. 107: pp. 1-9
- [16].Li, J., Li, Y., Xiong, L., et al., DC fault analysis and transient average current based fault detection for radial MTDC system. *IEEE Transactions on Power Delivery*, 2019. 35(3): pp. 1310-1320.
- [17].Li, Y., Wu, L., Xiong, L., et al., DC fault detection in MTDC systems based on transient high frequency of current. *IEEE Transactions on Power Delivery*, 2018. 34(3): pp. 950-962.
- [18].Tang, L., Dong, X., Shi, S., et al., A high-speed protection scheme for the DC transmission line of a MMC-HVDC grid. *Electric Power Systems Research*, 2019. 168: pp. 81-91.
- [19].Song, G., Chu, X., Gao, S., et al., A new whole-line quick-action protection principle for HVDC transmission lines using one-end current. *IEEE Transactions on Power Delivery*, 2014. 30(2): pp. 599-607.
- [20].Wang, X., Gao, J., Song G., et al., High impedance fault detection method based on variational mode decomposition and Teager-Kaiser energy operators for distribution network. *IEEE Transactions on Smart Grid*, 2019. 10(6): pp. 6041-6054.
- [21].Rosso, O.A., Blanco, S., Yordanova, J., et al., Wavelet entropy: a new tool for analysis of short duration brain electrical signals. *Journal of Neuroscience Methods*, 2001. 105(1): pp. 65-75.
- [22]. Tong, N., Lin, X., Li Y., et al., Local measurement-based ultra-high-speed main protection for long distance VSC-MTDC. *IEEE Transactions on Power Delivery*, 2019. 34(1): pp. 353-364.